

NuMI Primary Beam Design Report

P. Lucas, S. Childress, A. Drozhdin, J. Johnstone
6 December, 2002
Updated 28 April, 2003

Table of Contents

I.	Introduction	1
II.	Specifications	2
	• Positional precision and stability	2
	• Beam angle	2
	• Beam size	3
	• Loss levels	3
III.	Beamline elements	3
	• Kicker	3
	• Extraction region	6
	• Beam transport and targeting	7
	• Layout	10
	• Focusing sensitivity	14
	• Trajectory sensitivity and correction	16
IV.	Aperture analysis	17

EDITOR'S NOTE: The purpose of this document is to describe the physics design of the primary beamline. Related subsystems: controls, beam instrumentation, permit system, water, vacuum, are described elsewhere.

I. Introduction

The first element in the production chain of NuMI neutrinos is the 120 GeV primary proton beam. This beam is extracted from the Main Injector and transmitted roughly 1200 feet to an underground target hall. The chief criteria which have guided the design of this beamline have been transmission of high intensity with minimum losses and precision of targeting.

The beamline specification calls for the transmission of a 4×10^{13} proton pulse every 1.9 seconds. While generation of this intensity is not yet possible in the accelerator complex, 50% of it is achievable at present and upgrades are being planned to reach, or exceed, the specified value. At the design intensity, NuMI would use each year a number of protons comparable to that accelerated in Fermilab's entire history to this point.

There are problems associated with transmission of such an intense beam, chiefly associated with the necessity of maintaining minimal losses. The chief concerns are those of activating components and, due to the location of the beamline, contaminating groundwater. If a significant amount of beam, of order one percent, were chronically lost in any region of the line, the components in that region would be activated to a level of greater than 10 rads per hour, making maintenance problematical.

Typically groundwater contamination has not been a problem at Fermilab. This is because the water has been situated many feet below the level of beamlines and accelerators. Basically, in the time taken for any radionuclides to migrate down to the level of an aquifer, several half-lives will have passed and the activity will have been greatly reduced. However for NuMI the primary beam is transmitted to and into the aquifer region. Thus the decay time argument does not apply and the loss criteria are made much more stringent.

There is one advantage to having a beam so far beneath the surface. Namely the overburden naturally present is sufficient to shield the surface from prompt radiation from below. Thus no berm is required above any new NuMI tunnels.

The criteria for targeting of the proton beam, specified in detail below, are not unprecedented. However they are nonetheless severe. The one feature which is new is the requirement to point the beam accurately at a distant location, namely the Soudan mine. The secondary hadron and neutrino beams are produced at zero degrees relative to the proton beam and thus it is imperative that the proton beam be accurately directed at Soudan at the point of targeting. Since the primary signature of neutrino oscillations is a shortage of muon neutrinos at the far detector, it is imperative to assure that no deficit arises due simply to poorly aimed beam.

The evolution of the design of the line is worthy of comment. There are bend strings in three locations – the MI60 region of the Main Injector, the northeast extraction enclosure (NuMI stub) and the pretarget region immediately upstream of the NuMI target. The original design concentrated all beamline components in these same three regions. There

were long drift spaces of a few hundred feet each between MI60 and NuMI stub and again between stub and pretarget. The early concept was that installation of components between MI60 and the stub would obstruct the MI tunnel in a sensitive region. Between the stub and pretarget the original plan was to construct by microtunneling techniques a tunnel only large enough to contain a beam pipe, with no room for other components. This region has been referred to as the 'carrier tunnel.' The microtunneling idea was abandoned early in the project, and this region was constructed with much more material excavated than had originally been envisioned.

In fact it is seen that installation of additional components in the MI tunnel does not present insurmountable problems. Similarly, part of the carrier tunnel can also be occupied. The upstream half of this tunnel, that part which is constructed in soil, is round six feet in diameter - it would still be difficult to install components in this region. The downstream half, in solid rock, is ten feet wide and six feet high - components fit easily into it. The placing of components, specifically quadrupoles, in the previously unoccupied regions led directly to a much more manageable beamline, with smaller quadrupole currents and tighter focusing.

II. Specifications

The specifications established for the proton beam are as follows.

- Positional precision and stability The position specification on the target is established by the physics of the experiment as 0.5 mm. The instrumentation specified will be adequate to fix the beam center within $\pm 100\mu$ and the program Autotune will be used to maintain the position to high precision. The target multiwire will be used in determining this position and it must be surveyed accurately. Detectors downstream of the target (hadron detector, muon detectors, neutrino near detector) will also be used in establishing that the beam is accurately on target. The position stability upstream of the target is not fixed by physics. However variation which can be corrected to the 1 mm level is required by aperture considerations.

The level of concern over positional instability depends on how such instability occurs over time. If a variation happens over minutes or hours it can be correctable to a certain level by tuning. If any instability were to be seen as a pulse to pulse jitter, correction would not be possible. A more detailed discussion of stability, in particular in how it pertains to power supply regulation, is found below in the subsection on trajectory sensitivity and correction.

There will be some variation of the MI central momentum, perhaps as high as the present upper limit of .05%. Insofar as the horizontal or vertical dispersion function at the target is non-zero there will be position shifts there, and target dispersion functions are thus limited to $\sim .6$ meters in magnitude.

- Beam angle Assigning an appropriate fraction of the angle error budget, as determined from physics, to the primary beam, yields a required precision of 60 μ rad at

the target. The final two instrumentation stations are located 12.5 m apart, so that a 1 mm relative position error between them will lead approximately to 80 μ rad. The instrumentation itself will operate with a precision of an order of magnitude better than this 1 mm value, so that the real limitation will be on the relative alignment of two detectors.

- Beam size The beam spot on target is to be round with a σ of 1 mm. A different size might be specified for a beam intensity different from the nominal 4×10^{13} protons per pulse. For comparison purposes, the target is rectangular in shape with a width of 6.4 mm and a height of 15.0 mm. The specification on the spot size is $\pm 10\%$.

Note that the transverse emittance of Main Injector beam at NuMI intensities is not known with certainty. Thus quadrupole settings have been determined for values of 20π , 40π and 60π mm-mr (95%, normalized). It is also necessary that the spot size not change significantly over the 95.4 cm target length. If the limit is again set at 10%, this limits the magnitudes of the horizontal and vertical α (Twiss) parameters to ~ 12 . Note that there is also a contribution to the spot size from dispersive effects. If the momentum spread value were to be as bad as the present upper limit of .3%, this would limit the horizontal and vertical dispersion functions to .033 m. Similarly the dispersion slope functions must be such as to not allow the dispersive contribution to the beam size to exceed 10% over the length of the target.

- Loss levels Losses must be minimized as they lead to air activation, component residual activity and potential equipment damage. However the most stringent constraint for NuMI is, as was mentioned above, that of groundwater irradiation or contamination. Loss limits in different regions along the beamline have been determined; these limits vary due to the water flow rate, since water which flows more slowly will have the potential to be more highly activated. At elevations higher than that of the aquifer region the more familiar migration time to the aquifer plays a role. The most sensitive location is that where the carrier pipe traverses the interface between soil and rock. The fraction of beam loss in this, rather limited, region must be kept below a few $\times 10^{-6}$, or a handful of full intensity pulses in the average water residency time of four months. Note that the beampipe is specified as 12" in diameter in this region. It is difficult to devise scenarios in which a significant fraction of any beam spill hits this pipe; in particular upstream trim magnets do not have enough strength to do so. Although this interface region loss limit is the most stringent, any losses at or downstream of it will be serious. The more downstream locations, the pretarget hall and occupied parts of the carrier tunnel, with relative loss limits of 1.4×10^{-4} are in some ways more worrisome in that smaller beam missteerings in the stub could lead to striking components there.

III. Beamline elements

- Kicker The requirements on the extraction kicker were originally presumed to be similar to those of the long-batch kicker, which used to be operational at MI52. However experience with the existing systems and results of our own simulations indicate that a comparable configuration would be inadequate. The purpose of any extraction kicker is

Table 1 - Extraction Kicker Specifications
 (Most physics specifications from MI Note #258, 1/6/00 D.E.J.)

Physical & Good Field Aperture:	81 mm H x 33 mm V elliptical shape
Kick Angle @ 120 GeV:	950 μ rad to inside of ring
Field Rise Time (1%-99%):	1.30 μ s
Field Fall Time:	N/A
Field Flattop Time:	9.78 μ s minimum(6 batches)
Flattop Integrated Field:	3.8 kG - m
During Pulse:	\pm 0.5%
Pulse to Pulse:	\pm 0.5%
Repetition Rate:	1.9 seconds
Required Charging Time:	1.5 seconds

to develop a separation between circulating and extraction orbits at the face of a Lambertson magnet. The MI52 first Lambertson has been found to be quite highly activated, and our simulations show that indeed the two kicker configuration which precedes it does not provide enough kick to clear the septum cleanly. Since the NuMI extraction region must transmit roughly five times as much beam as MI52 does with a likely larger transverse emittance, it has been decided to construct three, rather than two, kicker magnet modules. The three magnets will together supply 3.8 kG-m of integrated field, and achieve adequate separation at the Lambertson.

The normal operating mode will be one in which five Booster batches, each consisting of ~82 18.9nsec bunches, are extracted, a single Booster batch having previously been sent to the antiproton source on the same accelerating cycle. However for periods when antiproton is not in a stacking mode it will be desired to extract six Booster batches to NuMI. This latter mode has essentially the same requirements as did six batch extraction to the Tevatron, which was effected by the MI52 long batch device. The specifications for the kicker system are given in Table 1.

There are two major changes required in designing the new magnets as compared to the existing ones. The rapid cycling of the kicker (1.9 second repetition rate) combined with the long pulse time lead to an increased duty factor and higher heat load. A polarity change is also required due to a 180 degree change in the phase advance from that used previously. A cross-sectional view of a kicker magnet is given in Figure 1. The magnets are to be located in the region downstream of quadrupole Q602 with the power supply upstairs in the MI60 South Power Supply Room.

A measured waveform from an existing kicker is shown in Figure 2. It is seen to satisfy the given specifications. However note that there is no criterion given in the specifications for fall time and that there is ringing after the pulse is completed. This feature implies that there can be no beam left in the Main Injector after NuMI extraction and thus that this kicker design is not satisfactory for any scenario in which NuMI beam is extracted first on any given cycle, with extraction to antiproton following.

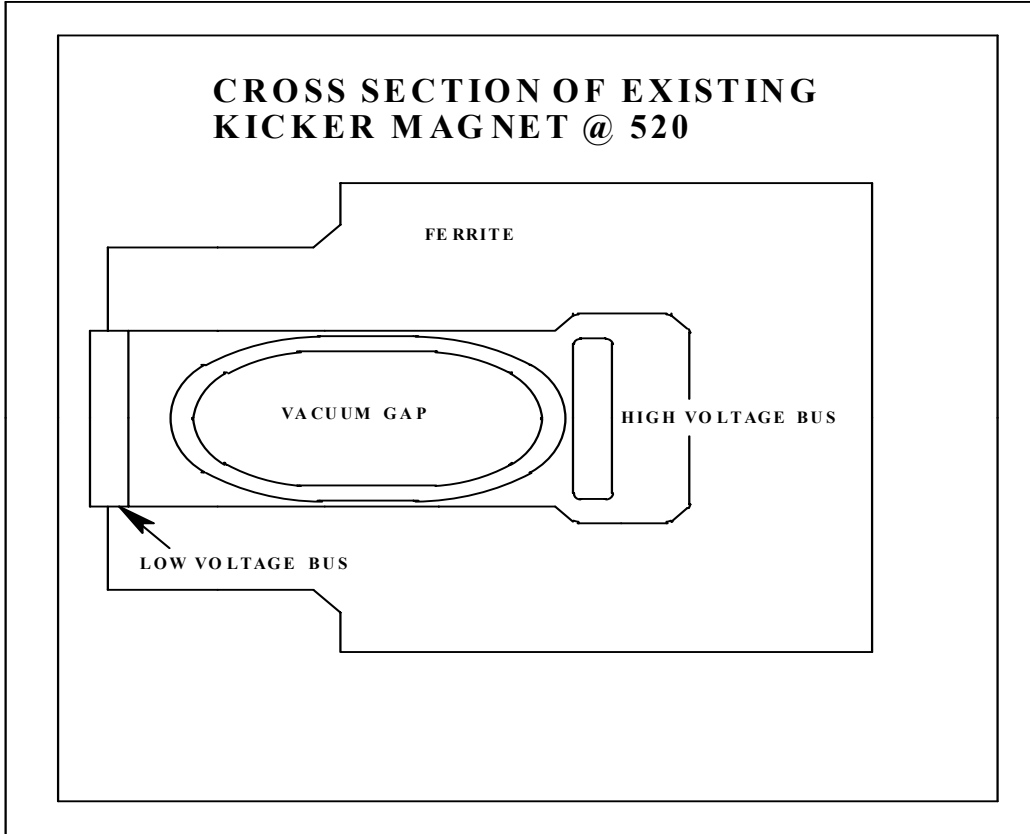


Figure 1: Kicker magnet cross section

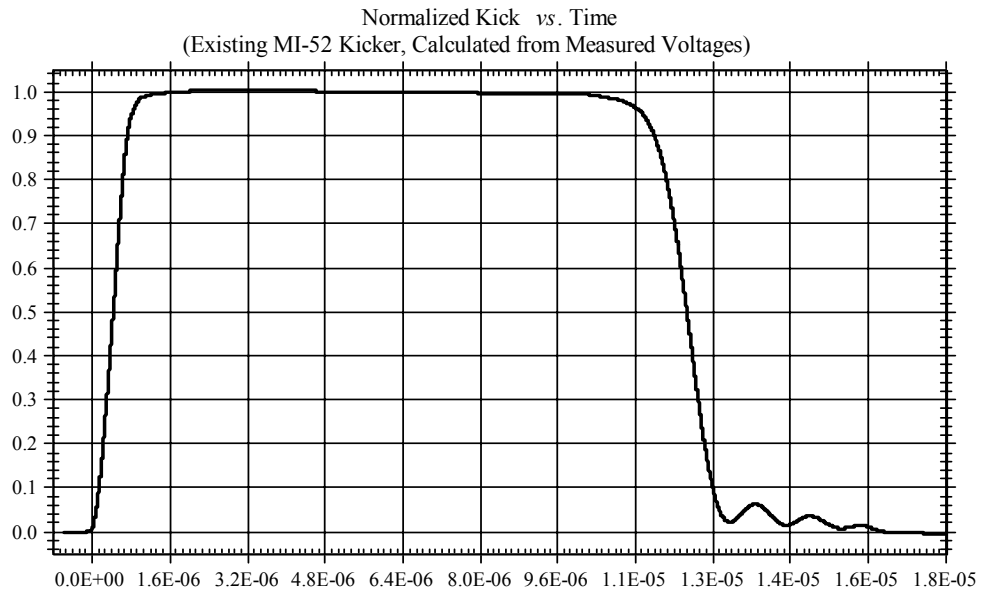


Figure 2: Measured MI52 long-batch kicker waveform

Table 2 Extraction Parameters

Quadrupole displacements: (x positive is toward the outside of the ring)

Q602: X = 3.1 mm
Q606: X = -.55 mm
Q608: X = -3.9 mm
Q610: X = -3.7 mm
Q612: X = -3.4 mm

Horizontal corrector fields at extraction:

H602: B = -.726 kG
H604: B = -.039 kG
H606: B = .208 kG
H608: B = 1.341 kG
H610: B = 1.427 kG
H612: B = 1.509 kG

Lambertson fields & septa positions:

LAM60A: B = 5.324 kG; X = 2.0 mm, Y = -1.5 mm, rotation = .145 radians
LAM60B: B = 10.734 kG; X = 2.0 mm, Y = 0, rotation = .020 radians
LAM60C: B = 10.734 kG, X = 2.0 mm, Y = 0, no rotation from vertical

There was for a time during the design period a fear that it would not be possible to obtain the ceramic beam tubes which are necessary within the kicker magnets. There was some R&D into nonconducting materials other than ceramic, should a change have been required. However appropriate ceramic devices were recovered from existing magnets.

- Extraction region The primary active elements for extraction are the three Lambertson magnets. The methodology followed for establishing beam orbits in the MI60 region, where these magnets are located, is as follows. A horizontal excursion of the circulating beam is established, primarily by offsetting several quadrupoles; the required displacements are given in Table 2. Once extraction energy has been approached and beam size has decreased, corrector magnets are used to make an additional contribution to the excursion; Table 2 includes the fields. The bumps are all constructed to be local so that the circulating beam is unaffected outside the extraction region. With the circulating beam on its 'extractable' orbit the kicker is fired and creates an extraction bump extending from location 602 through 608 and terminating in the field region of the Lambertsons.

A complication of all the MI extraction regions is that the strongly focusing MI lattice requires that a quadrupole, in our case Q608, be placed between the Lambertsons. One effect is that the extracted beam passes through this magnet off-center (in addition to the

magnet being displaced as part of the orbit bump) and sees considerable quadrupole steering. This steering must be counteracted by a horizontal kick from the Lambertsons and thus the first two are rolled to provide an outward deflection in what is primarily a vertical bend. A second problem is that the, primarily vertical, kick that Lambertson 1 generates makes the aperture of the quadrupole limiting on the beam which can be transmitted into the line. Due to this effect the first Lambertson is run at a reduced current, limiting its kick and the extracted beam excursion in the quadrupole. To effect extraction Lambertsons 2 and 3 must be run somewhat above their nominal value, though still within their specified current limit. Figure 3 shows the circulating and extracted orbits together with an expanded view of the 608 region. The clearances of the beam vs. septa and apertures in the extraction region are shown in detail below in Figure 12b, after the methodology involved in making such a plot is explained.

Figure 4 shows the results of a tracking study through the extraction channel. The quantity plotted is the fractional beam loss through the extraction region as a function of kicker strength. The losses on the left side of the figure, for too small kick, are found to occur primarily on the septum of Lambertson 1; while those on the right, for too strong kick, occur on the Q608 aperture. The chosen strength of 3.8 kG-m is well centered in the minimal loss region.

The final extraction element is a standard MI C-magnet, installed as a pure vertical bend and positioned as far upstream as possible given physical constraints, the most crucial of which is achieving sufficient vertical displacement above the MI beam level.

- Beam transport and targeting The beam transport consists of three bend regions as mentioned above together with quadrupole focusing in the straight sections connecting them. The quadrupole layout and design principles are discussed in detail in TM-2174 (May 28, 2002; John Johnstone, author). Some parts of that report are excerpted herein. Table 3 presents all of the elements of the line.

There are 21 quadrupoles, the first 4 of which perform the optical match between the β 's and α 's of the MI to those appropriate to the line itself. Through this section β is kept small enough in both planes to avoid problems with tight EPB apertures. The matching section is followed by 86 m of FODO cells characterized by quads Q105 – Q109. The half-cell length and phase advance are such that this part of the line closely replicates the MI lattice. Quads Q110, Q111 and Q112 at the upstream end of the carrier pipe and Q113, Q114 and Q115 at the downstream end create long straight section optics. The peak β 's in the doublets are equal at ≈ 125 m.

The last 6 quadrupoles in the line form the final focus optics to obtain the desired beam size at the target and also to eliminate vertical and insofar as possible horizontal dispersion there. With the vertical bends required, it is not simple to fix $\eta_y \approx 0$ over any appreciable range of extracted MI beam emittances. With $\beta_{x\max}$ and $\beta_{y\max} \approx 100$ m, aperture restrictions are not an issue through this region. The final focus segment is

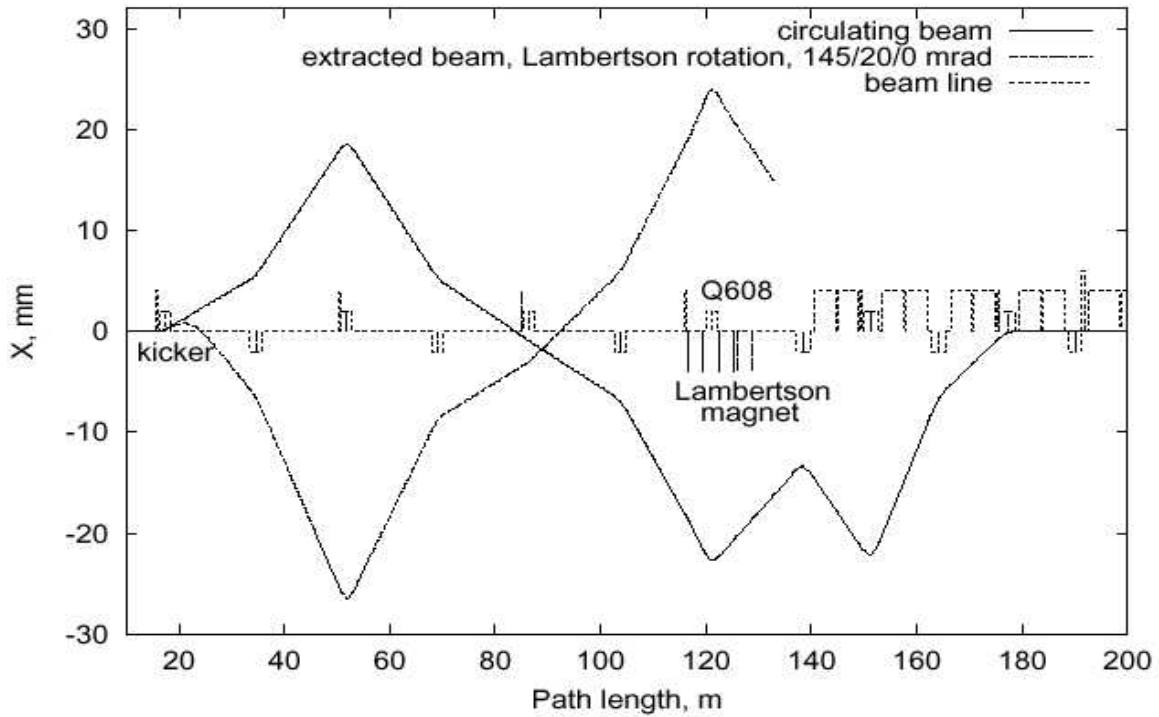


Figure 3a. Circulating and extracted beam orbits in the MI60 region

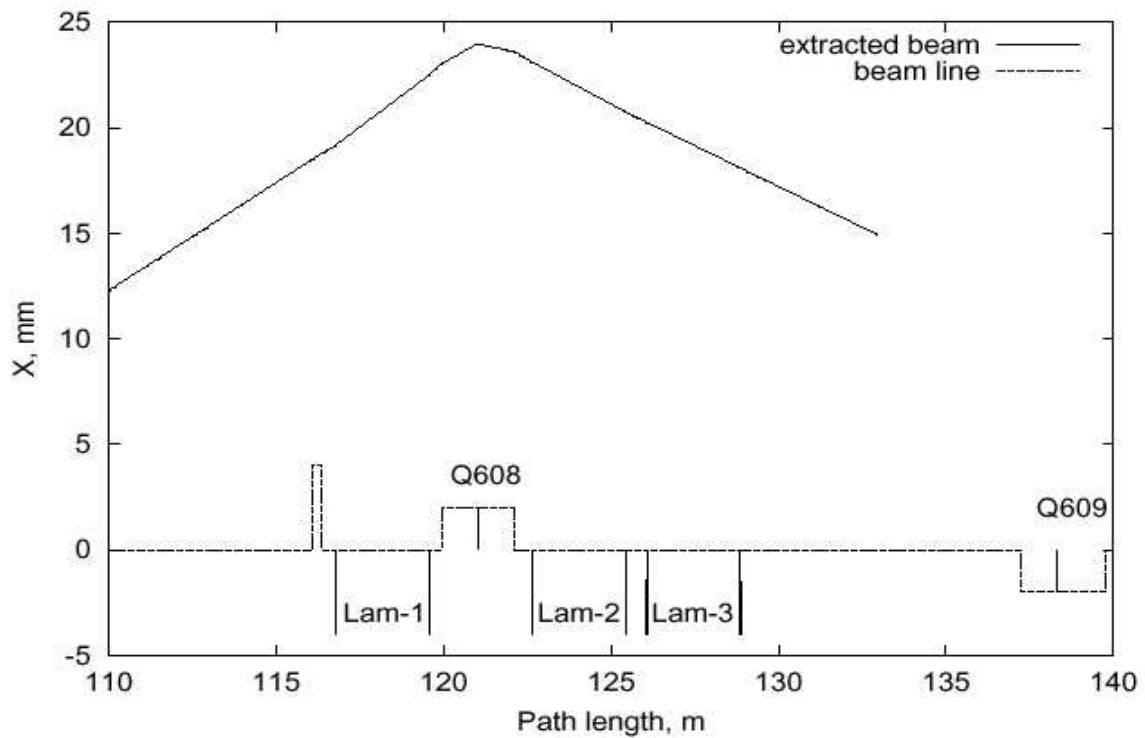


Figure 3b. Extracted beam orbit through Lambertsons

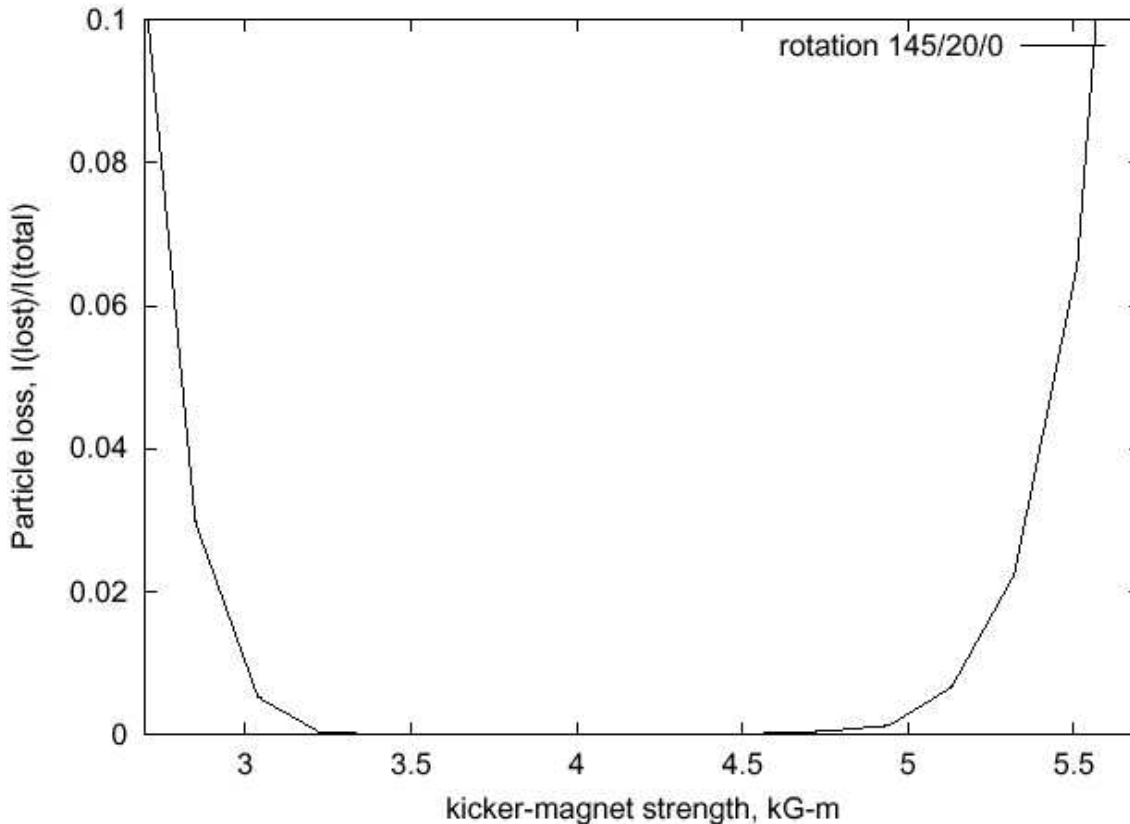


Figure 4. Extraction losses vs. kicker strength

Table 3 Components of the Primary Proton Line

<u>Element</u>	<u>Number</u>	<u>Purpose/Comment</u>
Dipoles:		
EPB	6	Transport in MI60 region
B2	10	Downbend in NuMI stub, upbend in pretarget
35" SY 'trim'	2	Trim in MI60 (provides a strong horizontal corrector in this area), 1 horizontal bend in pretarget
Quadrupoles:		
3Q120	17	Transport and targeting
3Q60	4	Transport
Trims:		
Horizontal	10	MI IDH correctors, two to have aperture increased from 1.0" to 1.5"
Vertical	9	MI IDH correctors rolled 90 degrees, two to have aperture increased from 1.0" to 1.5"
Beam instrumentation:		
Horizontal BPMs	13	Two nearest target to have double resolution
Vertical BPMs	11	Two nearest target to have double resolution
Multiwires	10	Two nearest target have .5 mm wire spacing, others have 1 mm wire spacing
Toroids	2	Measure intensity in line with some redundancy
Total loss monitors	4	Integrate losses over major beamline sections
Sealed loss monitors	35	Localize any loss points

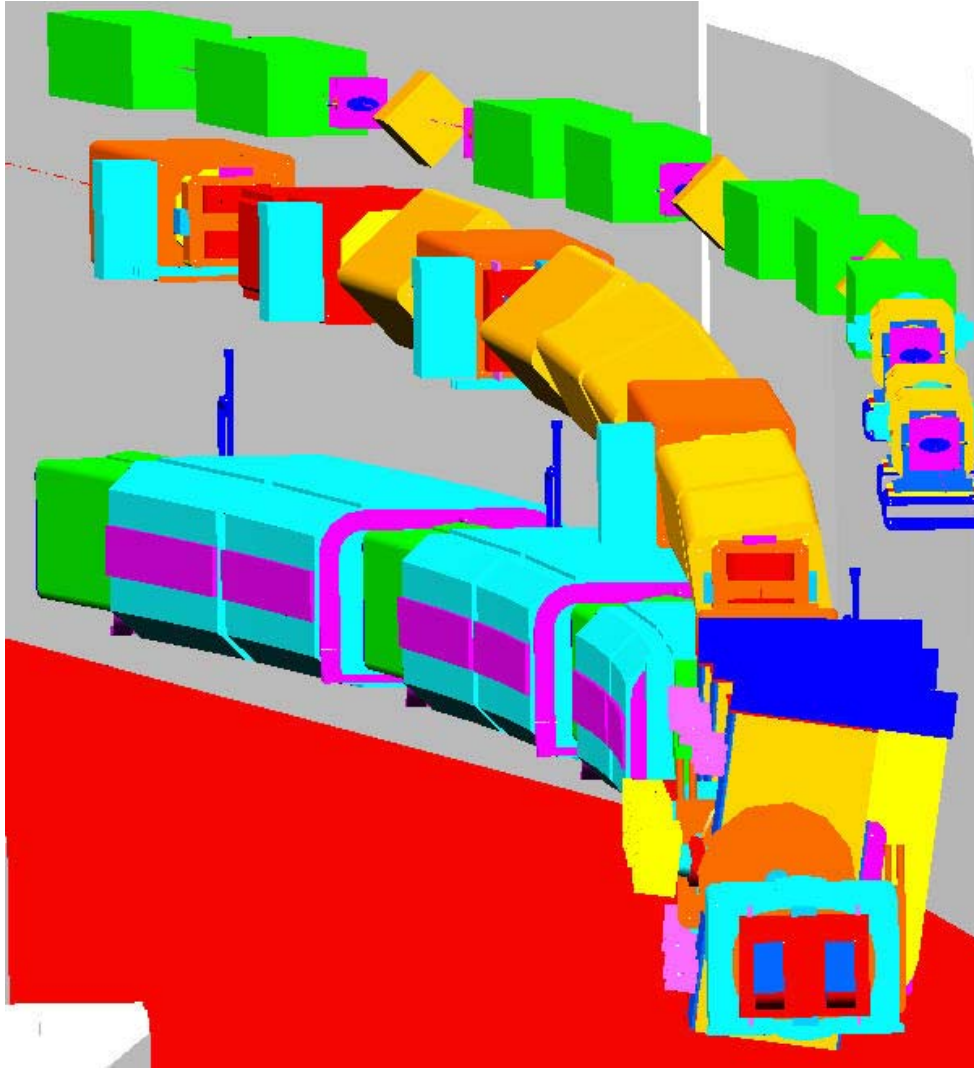


Figure 5a. The MI60 region, of the NuMI beamline. The MI ring is on the bottom, the Recycler ring is on the top and the NuMI line is between.

optically flexible and can comfortably accommodate tuning to at least $\pm 30\%$ β variations in each plane independently.

- Layout Figure 5a shows the extraction region (partially obscured) and the first beamline bend. It is seen that the NuMI line in this region fits comfortably between the MI below and the Recycler ring above. The bend in this region comes from a string of six EPB dipoles, powered in series to the design field of 15.0 kG but rolled at five separate angles. In the horizontal plane the deflection is such as to accomplish most of the horizontal bend required to hit Soudan, a small final bend in pretarget accomplishing the remainder. (In the original design this EPB string provided all of the required horizontal bending. However sufficient developments occurred that it became impossible to adjust both the horizontal position and angle at the target using just this string.) In the vertical the goal is to have the beam exit this region level, or nearly so, so as to avoid generating

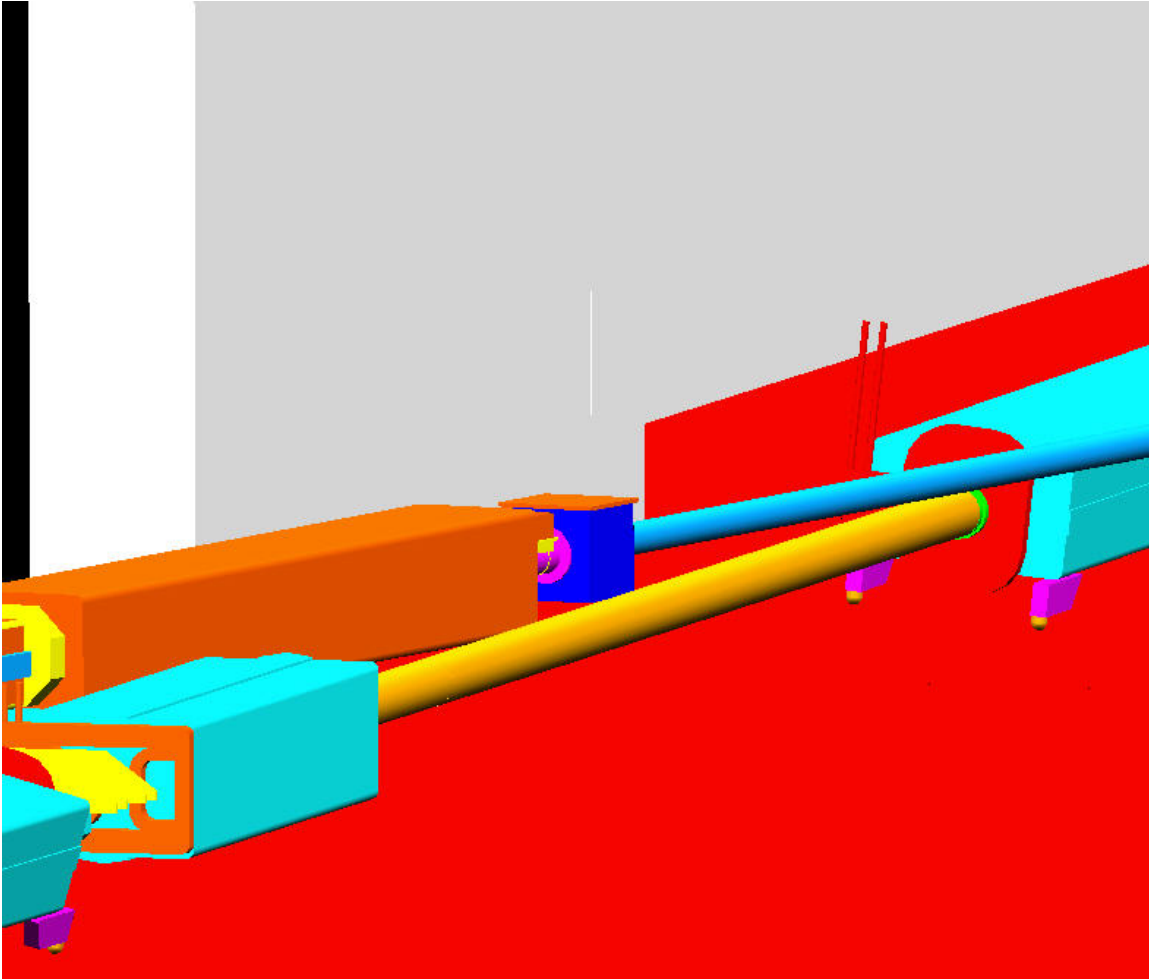


Figure 5b. View of the region where the NuMI beamline passes above the A150 line

interferences with existing equipment. The actual pitch angle achieved is -0.27 milliradians.

The last potential interference is with the A150 line, that which carries 150 GeV antiprotons from the MI to the Tevatron. The NuMI line crosses this one somewhat downstream of the MI60 region. Figure 5b indicates reasonable clearance at this location.

To be directed toward Soudan vertically it is necessary to bend the protons at a pitch of -58 milliradians. What is actually done is to bend by -156 milliradians, the goal being from a civil construction standpoint to descend below clay soil into bedrock as soon as possible, and then to bend back $+98$ milliradians to set the final pitch. The downbend occurs in a region known as the northeast extraction enclosure (NuMI stub), basically an alcove-like extension of the MI60 straight section. This region and the beamline in it are pictured in Figure 5c. It is seen that there are three separate floor elevations. The upper two levels were built as part of the MI construction, while the lowest was added by the NuMI project. The downbend is accomplished by a string of six Main Ring B2 magnets,

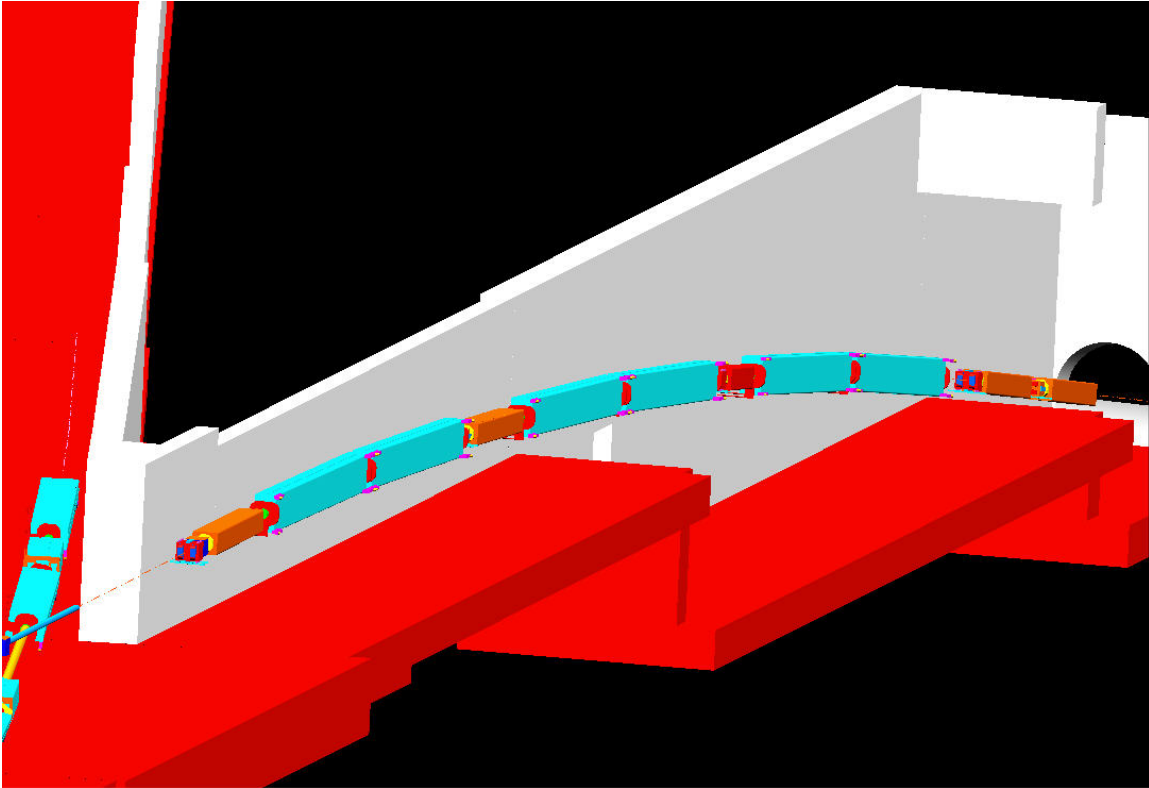


Figure 5c. View of the NuMI beamline as it traverses old (upper levels) and new (lowest level) regions of the MI northeast extraction enclosure (NuMI stub)

rolled by 90 degrees. The bend field of 17.1 kG is safely below the design value of 17.8 kG.

If left uncompensated this major downbend would generate a significant vertical dispersion. A major accomplishment of the optics design is that dispersions are kept reasonable throughout. Immediately downstream of this stub area is that part of the carrier region which is still unoccupied by beamline components.

Figure 5d shows the downstream end of the beamline, the upbend and the focusing region which takes beam to the target. Also present here is the small horizontal bend (.40 milliradians) necessary to hit the target while simultaneously having beam directed toward Soudan. This is effected by a 35" Switchyard trim dipole. The major upbend here is again achieved by rolled B2 dipoles, in this case running at 16.1 kG.

A feature to note, which is not indicated by the figure, is that there is a considerable drift space, nearly 23 meters in total, from the last magnet to the target. Some of this space is inside the shielding pile and is reserved for an upstream move of the target if the need ever arises to change the secondary beam focus and raise the neutrino energy. Also inside the shielding is a graphite collimator, or baffle, whose purpose is to protect the target water system and the focusing horns from errant primary beam. If the primary beam were steered significantly off the target, it would proceed downstream beyond the target and

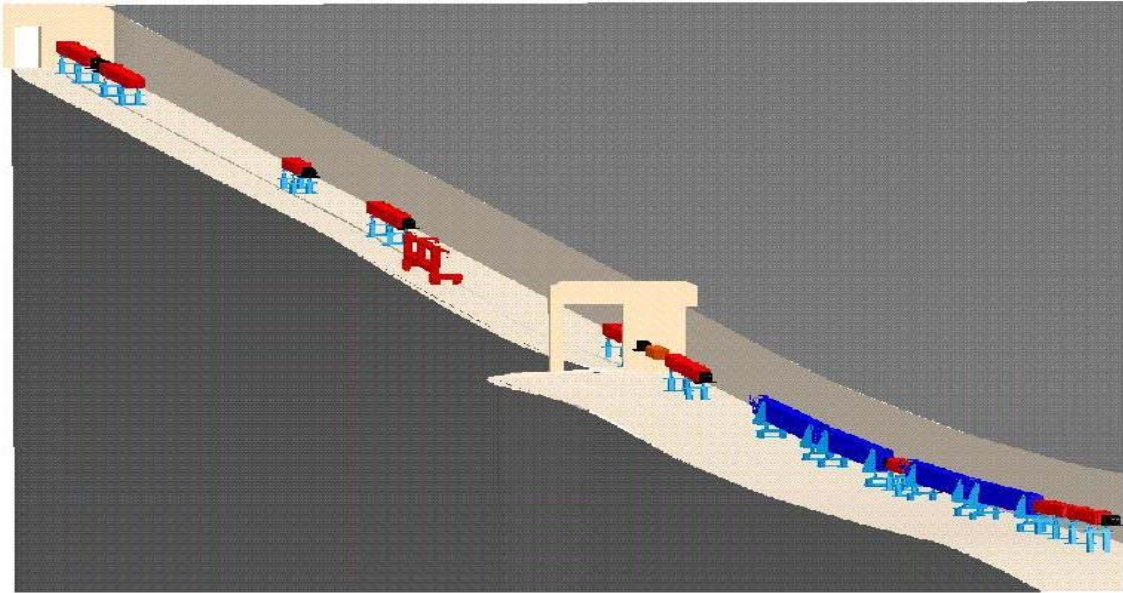


Figure 5d. View of the NuMI beamline in the pretarget region

would pose a real danger of impinging on a horn neck, particularly that of horn 1. The purpose of the baffle is to prevent this from happening. Similarly protected are the tubes which carry cooling water along the top and bottom edges of the target.

Included in Table 3 is a listing of the instrumentation of the beamline; basically the entire line is thoroughly instrumented. Firstly are position/intensity monitors associated with essentially all of the quadrupoles. With the transfer functions between trims and their corresponding BPMs known, these devices provide enough information to allow the steering of the line to be corrected throughout. Half of the quadrupoles also have associated multi-wire profile monitors. These are sufficient to assure that the line's focusing is as desired. Existing multi-wire versions intercept and scatter enough beam that they cannot remain in place during high intensity running. Tests are underway to determine if thinner and lighter wire can be used to remedy this situation. The locations of the profile monitors are indicated in Figure 11 below.

Other elements of instrumentation are sealed unit and total loss monitors and toroid intensity monitors. The purpose of the sealed units is to localize accurately any loss which might occur. The total loss monitors give a quantitative measure of total losses in the stub region, carrier tunnel and pretarget hall. The toroids provide a redundant measure of the total beam delivered. Together with a similar device in the MI ring, they assure that all circulating beam indeed arrives in the line and is transmitted to the region of the target. The region just upstream of the target is instrumented particularly well. 14.25 meters of the pretarget drift space is outside the shielding and is available for instrumentation. At the upstream end of this space is a complete instrumentation station,

with horizontal and vertical BPMs and a profile monitor. Each of these instruments is specified to have double the accuracy of the ones in the transport region. Similar instrumentation is placed at the downstream end of the free space, with the downstream toroid added. Such good instrumentation at two separate locations allows the proton beam direction on target to be measured quite accurately, assuring that the protons, and thus the secondary mesons and neutrinos, are directed toward Soudan. The target profile monitor is also crucial for ascertaining the beam spot size near the target. This is important as beam will begin to miss the target in the horizontal direction if its width becomes significantly larger than the specified 1 mm sigma.

Focusing sensitivity The sensitivity of the optics to different error sources has been studied in simulations. Assigning random gradient errors of $\sigma(\Delta B'/B') = 25 \times 10^{-4}$ to the 21 quadrupoles in the line, Figure 6 shows the relative β -waves resulting from 20 random generator seeds. The β -wave accumulates progressively down the line of course, but $\Delta\beta/\beta$ never exceeds $\approx 10\%$, which translates into a maximum increase in beam size of $\approx 5\%$. This feature is confirmed by the results shown in Figure 7 where, for the same 20 seeds, the changes in σ 's are demonstrated to be less than ≈ 0.1 mm. At the target the maximum changes in beam size are on the order of only 0.05 mm, well within the specification.

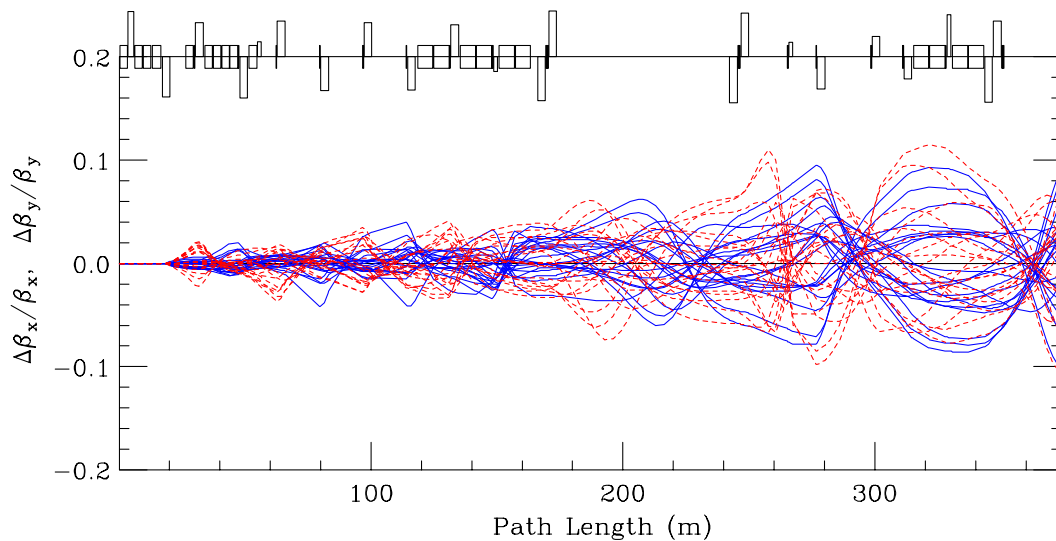


Figure 6. The effect on β due to random gradient errors with $\sigma(\Delta B'/B') = 25 \times 10^{-4}$

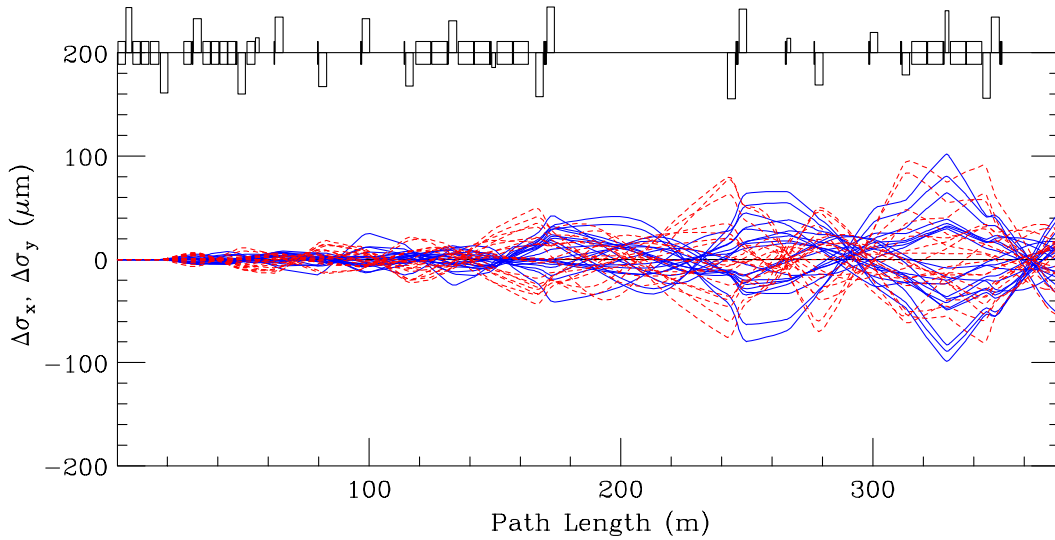


Figure 7. Beam size variation resulting from random gradient errors

Optical errors also arise from discrepancies between the assumed ideal and actual MI lattice functions. Figure 8 shows the β -envelopes that result from $\pm 10\%$ variations in the nominal β_x and β_y injection values¹. The upstream matching section can be re-tuned to eliminate these mismatches, but it can also be seen that this might not be strictly necessary – the maximum β 's are sufficiently well-behaved that no aperture problems arise, and the small residual mismatch at the target can be corrected with the four final-focus quadrupoles.

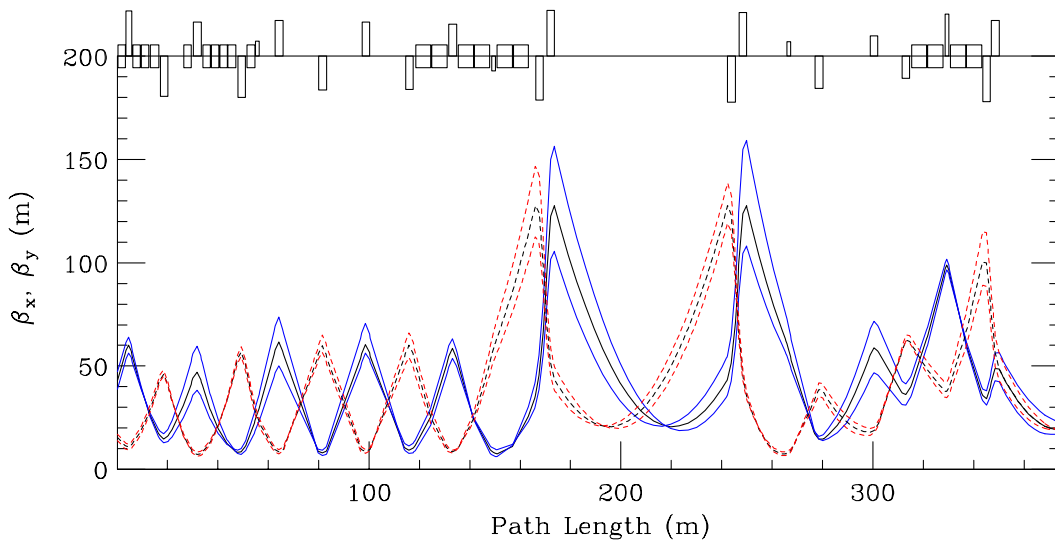


Figure 8. β -waves due to $\pm 10\%$ injection optic errors

¹ There is reason to believe that MI β errors are corrected (or certainly can be) to $< 5\%$ through tuning of the 53rd harmonic quadrupole circuits. For details, see; J.A. Johnstone, "A Numerical Simulation of Resonant Extraction", MI-0095, 1993.

Trajectory sensitivity and correction In addition to a BPM, as noted above, every focusing element in the line, with the exceptions of Q101 and Q104, also has an MI-style dipole corrector nearby. Space limitations at Q101 preclude installing a corrector there, while at Q104 a corrector would be redundant with those in both planes already nearby at Q103 and Q105. Orbit correction is an issue which, of course, must be addressed by any beamline, but for the ultra-clean transport requirements of NuMI it is critical that precise position control be available throughout.

Correction of central trajectory errors has been simulated with dipole field errors and random misalignments assigned to the beamline elements (including BPM's). Suitable error values are $\sigma(\Delta x, \Delta y) = 0.25$ mm, $\sigma(\psi_{roll}) = 0.50$ mr, and $\sigma(\Delta B/B) = 10 \times 10^{-4}$. Figure 9 shows the deviations from the central trajectory arising from 20 random error seeds. The uncorrected offsets in the line are $\Delta x(rms) = 2.63$ mm, $\Delta x(max) = 13.03$ mm, and $\Delta y(rms) = 2.33$ mm, $\Delta y(max) = 11.90$ mm.

That the deviations are virtually the same in the 2 planes indicates that quadrupole misalignments are the dominant sources of error. A 15 T/m quadrupole displaced transversely by 0.25 mm produces a kick $\sim 30 \mu r$, which is larger than the error angle created by $\Delta B/B = 10 \times 10^{-4}$ in any of the line's dipoles. In addition, there are more quadrupoles than dipoles.

The position errors used in this discussion are, as was stated, .25mm. There is concern, however, that the NuMI positioning errors will be greater, at least originally, in which case trajectory errors will scale accordingly.

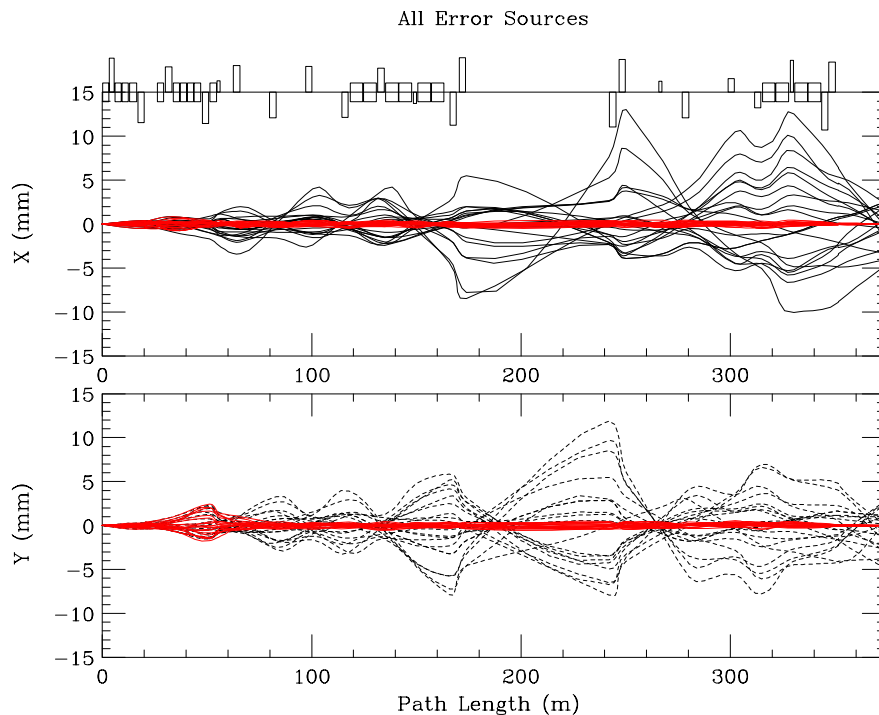


Figure 9. Uncorrected and corrected trajectories with random misalignments and dipole field errors

The corrected orbits from the above analysis are also shown in Figure 9 (in red). After correction the trajectory deviations are reduced to $\Delta x(\text{rms}) = 0.22$ mm, $\Delta x(\text{max}) = 0.85$ mm, $\Delta y(\text{rms}) = 0.36$ mm, $\Delta y(\text{max}) = 2.44$ mm, and the beam position and angle at the target are tuned to $\Delta x = \Delta y = 0$ mm, $\Delta x' = \Delta y' = 0$ μr . Maximum x and y deviations occur at Q102 and Q103, respectively. This is a reflection of the fact that position control at those locations requires tuning the MI kickers, Lambertsons and C-magnet – refinements not included in the present simulations.

The strengths required for trajectory correction are $\theta_x(\text{rms}) = 27.57$ μr , $\theta_x(\text{max}) = 91.55$ μr , and $\theta_y(\text{rms}) = 32.00$ μr , $\theta_y(\text{max}) = 95.21$ μr . Horizontal values are comfortably below the 150 μr design value available at 120 GeV/c. The maximum vertical kick, however, exceeds the maximum 75 μr attainable from a MI-style vertical corrector, and for this reason it has been decided to use rolled horizontal correctors in the vertical plane.

The sensitivity of the line to possible dipole mispowering is a subject of considerable interest and is now presented in greater detail. Figure 10a shows the situation for the horizontal plane and Figure 10b for the vertical. What is plotted is, for each bend supply, the effect on downstream beam positions of a .1% power supply drift of the peak current. Comparing with the specification of <0.5 mm for target position (the target is located at station 356 meters), it is seen that at least the major up and down bends will need regulation considerably greater than that used in making the figure. Taking into account the specification for stability along the beamline, the EPB string also requires more regulation. Table 4 provides a listing of power supply stability specifications. These are accomplished via techniques in use elsewhere in the laboratory.

IV. Aperture analysis

Figure 11 shows the amplitude (root β) and dispersion (η) functions over the entire line. The beam size peaks at stations 150 m and 225 m are at the upstream and downstream ends of the carrier tunnel. Putting relatively large betas at these quadrupoles allows the betas upstream and downstream of them to be appropriately small. Nominal design gradients have been kept to ≤ 16.0 T/m to enable safe DC operation, if desired, for the quadrupoles, and the optics have had some minor modifications made to them to allow this condition to be met.

Figure 12a shows the clearances vs. beam size over the entire line and Figure 12b shows an expanded view of the same in the Lambertson region. Considerable effort has gone into having a design for which this plot demonstrates adequate clearance over the length of the entire beamline, and several of the plot's features are worthy of detailed discussion.

- The aperture, or preferably clearance, shown for each element is the actual half-aperture of the device minus any sagitta in that device. Note that the entire sagitta is subtracted from the half aperture – this is appropriate given the way the magnets will be aligned. The B2 magnets have a camber of 86 mils along the direction which will be for us the horizontal. The purpose is so that when the magnets are installed in their normal configuration, rolled ninety degrees from ours, gravity will cause the centers to sag and

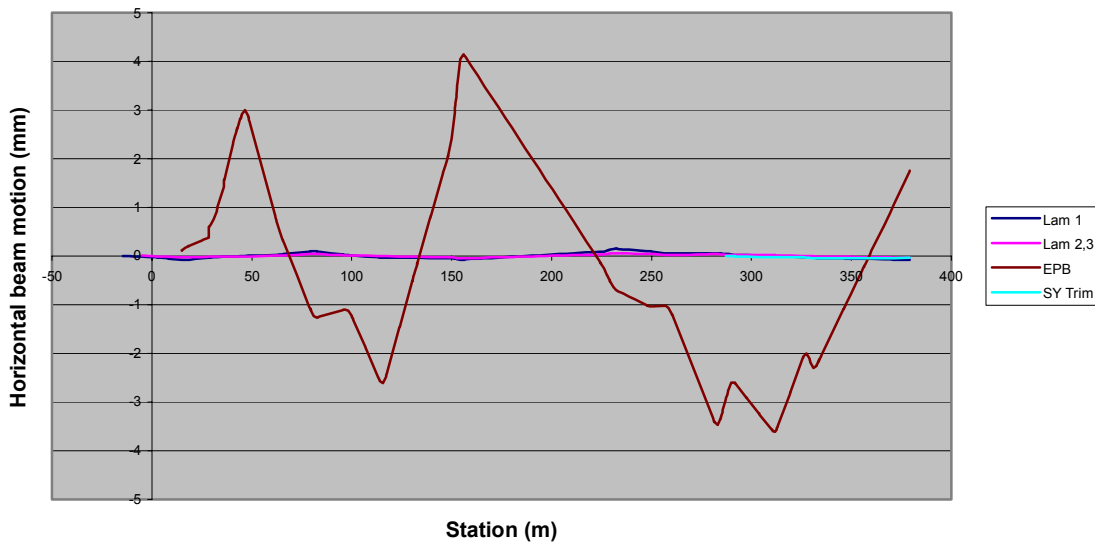


Figure 10a. Sensitivity in the horizontal plane to dipole power supply variations

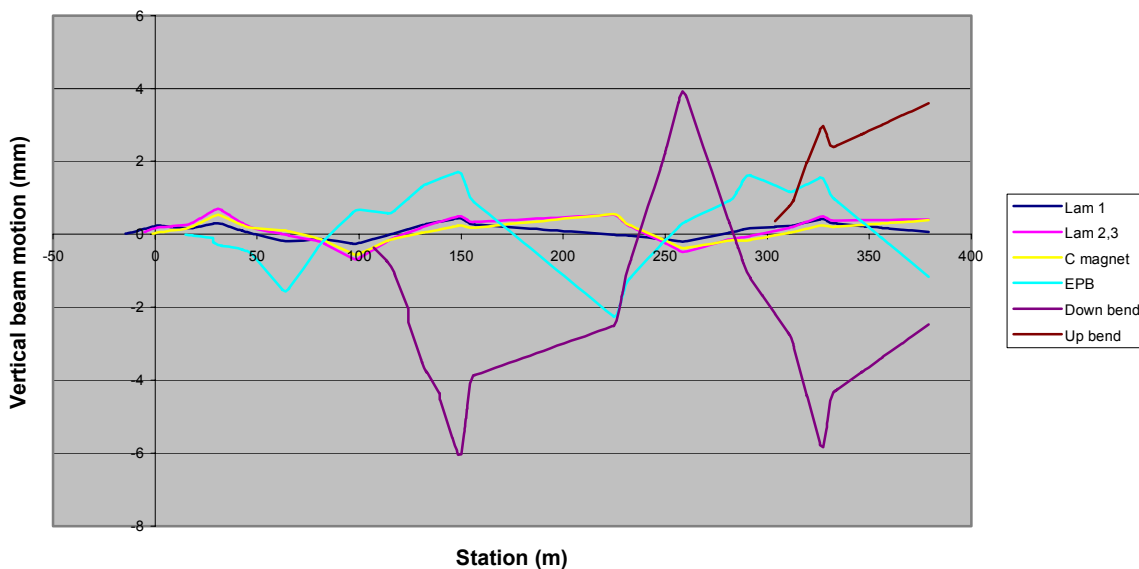


Figure 10b. Sensitivity in the vertical plane to dipole power supply variations

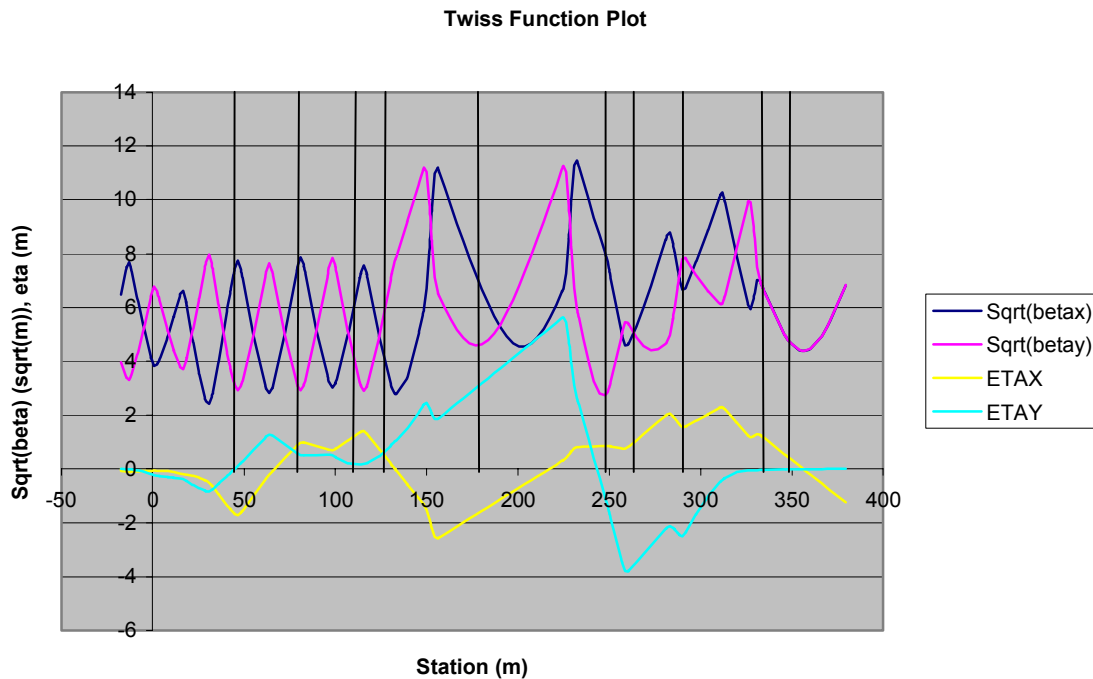


Figure 11. Amplitude and dispersion plots over the entire beamline. The target station value is 356 meters. The vertical lines represent the locations of profile monitors.

remove that camber. Thus for the B2s we lose clearance in the vertical direction due to sagitta and in the horizontal due to this effect.

- What is shown as clearance for the Lambertsons, and for MI quadrupole 608 which lies between Lambertsons 1 and 2, is worthy of special comment. The alignment of each of these magnets is determined by the path of the circulating MI beam, not the extracted beam. Thus the effective clearance is the distance from the beam center to the nearest aperture restriction, which for all Lambertsons is the septum. Note that the tighter clearance is in the horizontal plane and that, since the first two Lambertsons are rolled, the horizontal distance to the septum is dependent on the height of the beam. Secondly, since the magnets are aligned along the circulating beam direction, the extracted beam is not traveling parallel to the septum face. Both of these effects have been accounted for in making the plots, which have what appear as angled magnet apertures but which really are angled beam trajectories. Similarly for the case of Q608, what are plotted as clearances are horizontal and vertical distances to the edge of a star shaped vacuum chamber.

- As to the beam size plotted, there are curves for ‘beta’ size, ‘eta’ size and ‘total’ size. For beta, or emittance size, what is given is the contour for 500π in horizontal and vertical planes. This 500π value is determined by the restricted space seen by the circulating MI beam as it passes the complement of Lambertson magnets. In the arcs, where dispersive contributions inflate the beam size, a 500π emittance coupled with a momentum spread of $\delta p_{100}/p \approx \pm 7 \times 10^{-3}$ completely fills the machine aperture and,

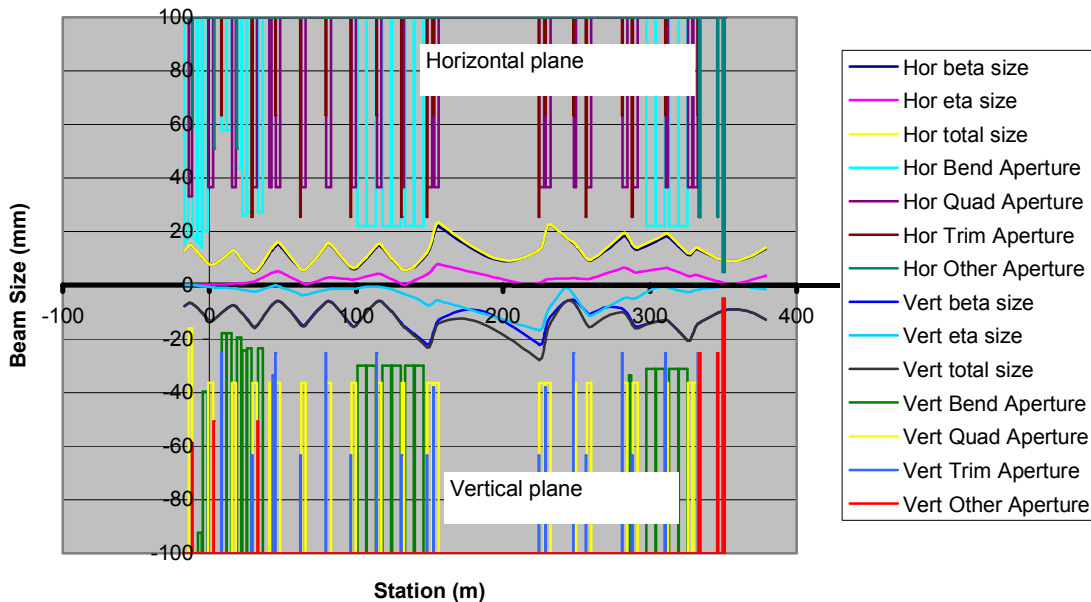


Figure 12a. Beam and aperture clearance plot over the entire beamline

Clearances in Lambertson Region

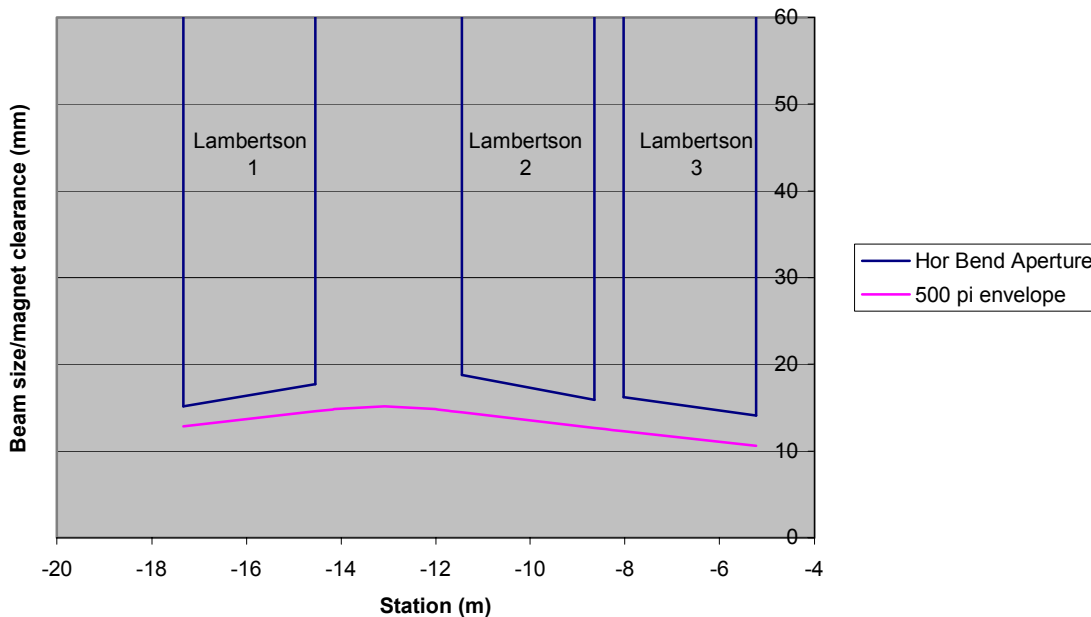


Figure 12b. Beam and aperture clearance plot in extraction region

therefore, defines the MI *admittance*. This admittance value for the momentum spread, however, is not a sensible value to use for NuMI. The RF bucket area at 120 GeV/c is ~ 10 eV-sec, whereas a $\delta p_{100}/p = 7 \times 10^{-3}$ translates into a longitudinal emittance of $\sim 50\text{--}60$ eV-sec and so could not possibly be maintained as it doesn't fit in the bucket. The maximum spread that can be contained by the RF is $\delta p_{100}/p$ of $\sim 3 \times 10^{-3}$ and this is the value used in making the figure. The total beam size is formed by adding the beta and eta sizes in quadrature. The significance of the envelopes shown in the figure, therefore, is that the ability the NuMI line to transport, without losses on any apertures, the worst quality beam that the Main Injector could conceivably spew forth is demonstrated. Note that the desired criteria at the target are met – the eta functions and slopes of beta functions are zero (as is the slope of the vertical eta function). Although it cannot be directly read from this figure, the sigma at the target of the 40π beam is the desired 1 mm.

- At station 350 m is an aperture through which the beam does not fit. This aperture is that of the horn protection baffle. The situation is that the optics are set in this figure to focus 40π beam on the target, while what is plotted is 500π beam. If beam were ever to become this large in practice, it would be considered errant and in danger of damaging one or both horns. Thus it is as designed that the horn protection baffle intersects such beam. If it were ever determined that beam considerably greater than 40π were desired to be transmitted, then the target focus would be made tighter and the apparent aperture restriction would not be present.

Table 4: NuMI POWER SUPPLY REQUIREMENTS															Current Regulation													
Ramp Cycle Time:		1.9													Est. I Ripple (720													
CIRCUIT(ACNET if different then CKT Name)	MAGNET TYPE	#	CABLE			PEAK CURR. (amps)	Min. Curr. (amps)	PEAK VOLT. (volts)	RMS CURR. (amps)	PEAK PWR (kW)	Power Supply				NO FILTER		"+/-" % of peak PS current, no extra reg.	"+/-" % of peak running current	Holec, FNAL elect. "+/-" % Max	"+/-" % of peak running current								
			#	TYPE	#						L	TYPE	Volt	Curr.	PS Loses	P-P amps					P-P %							
		MAGS	kcmil	1 way	(ft)					#, Man./Pwr	(volts)	(amps)	(kW)															
MI60 Power Supplies															\$10K/loop Filters (refurbished)		Cost:											
Kicker (I:KPS6N)	kicker	3																										
LAMB (I:LAM601)	Lamb.	1	500	2	132	765.85	0	200	400	153	1, Xrex/500kW	200	2500	4.00	1.23	0.16	0.100%	0.326%	0.010%	0.033%								
LAMB (I:LAM6023)	Lamb.	2	500	3	154	1806.3	0	200	794	361	1, Xrex/500kW	200	2500	7.94	0.63	0.03	0.100%	0.138%	0.010%	0.014%								
CMAG (E:V100)	Cmagnet	1	500	5	165	3482.5	0	50	1560	174	1, Xrex/500kW	50	5000	3.90	1.84	0.05	0.100%	0.144%	0.010%	0.014%								
E:Q101	3Q120	1	1/0	1	98	64.64	64.6	147	65	10	1, PEI/20kW	200	100	0.65			0.050%	0.077%										
BND1(E:HV102)	EPB	6	500	3	244	1645.7	0	600	914	987	3, Xrex/500kW	600	2500	27.42	0.37	0.02	0.100%	0.152%	0.010%	0.015%								
E:HT102	MI Corr.	1	10ga	1	197	25	0	147	14	4	MI DipoleTrim	150	30	0.11			0.100%	0.120%										
E:Q102	3Q120	1	1/0	1	148	64.64	64.6	148	65	10	1, PEI/20kW	200	100	0.65			0.050%	0.077%										
E:Q103	3Q120	1	1/0	1	206	72.36	72.4	167	72	12	1, PEI/20kW	200	100	0.72			0.050%	0.069%										
E:VT103	MI Corr.	1	10ga	1	267	25	0	151	14	4	MI DipoleTrim	150	30	0.11			0.100%	0.120%										
E:Q104	3Q60	1	1/0	1	225	33.68	33.7	56	34	2	1, PEI/20kW	100	200	0.17			0.050%	0.297%										
Earlyly		1	1/0	1	250	0	0	0	0	0	1, PEI/20kW	200	100	0.00			0.050%	#DIV/0!										
E:HT105	MI Corr.	1	10ga	1	301	25	0	153	14	4	MI DipoleTrim	150	30	0.11			0.100%	0.120%										
E:Q105	3Q120	1	1/0	1	253	60.04	60	139	60	8	1, PEI/20kW	200	100	0.60			0.050%	0.083%										
E:VT106	MI Corr.	1	10ga	1	358	25	0	156	14	4	MI DipoleTrim	150	30	0.11			0.100%	0.120%										
E:Q106	3Q120	1	1/0	1	310	60.04	60	140	60	8	1, PEI/20kW	200	100	0.60			0.050%	0.083%										
E:HT107	MI Corr.	1	10ga	1	414	25	0	160	14	4	MI DipoleTrim	150	30	0.11			0.100%	0.120%										
E:Q107	3Q120	1	1/0	1	366	60.04	60	141	60	8	1, PEI/20kW	200	100	0.60			0.050%	0.083%										
E:VT108	MI Corr.	1	10ga	1	471	25	0	163	14	4	MI DipoleTrim	150	30	0.11			0.100%	0.120%										
E:HT109	MI Corr.	1	10ga	1	527	25	0	167	14	4	MI DipoleTrim	150	30	0.11			0.100%	0.120%										
E:VT110	MI Corr.	1	10ga	1	583	25	0	170	14	4	MI DipoleTrim	150	30	0.11			0.100%	0.120%										
E:VT111	MI Corr.	1	10ga	1	646	25	0	174	14	4	MI DipoleTrim	150	30	0.11			0.100%	0.120%										
E:HT112	MI Corr.	1	10ga	1	662	25	0	175	14	4	MI DipoleTrim	150	30	0.11			0.100%	0.120%										
MI60N Power Totals:															48													
MI62 Power Supplies																												
E:Q108	3Q120	1	1/0	1	637	60.04	60	145	60	9	1, PEI/20kW	200	100	0.60			0.050%	0.083%										
BND2 (E:V109)	B2	6	500	8	624	4447	0	400	2360	1779	MR - type	470	5000	6.66	0.90	0.02	0.100%	0.112%	0.010%	0.011%								
E:Q109	3Q120	1	1/0	1	581	60.04	60	144	60	9	1, PEI/20kW	200	100	0.60			0.050%	0.083%										
E:Q110	3Q60	1	1/0	1	525	24.69	24.7	43	25	1	1, PEI/20kW	100	200	0.12			0.050%	0.405%										
E:Q111	3Q120	1	1/0	1	520	55.99	56	133	56	7	1, PEI/20kW	200	100	0.56			0.050%	0.089%										
E:Q112	3Q120	1	1/0	1	542	59.03	59	141	59	8	1, PEI/20kW	200	100	0.59			0.050%	0.085%										
MI62 Power Totals:															9													
															minus MR PS/Xformer													
Upstream Service Building and Horn Power Supplies																												
E:Q113	3Q120	1	1/0	1	732	59.03	59	144	59	8	1, PEI/20kW	200	100	0.59			0.050%	0.085%										
E:VT113	MI Corr.	1	10ga	1	701	25	0	177	14	4	MI DipoleTrim	150	30	0.11			0.100%	0.120%										
E:HT114	MI Corr.	1	10ga	1	692	25	0	177	14	4	MI DipoleTrim	150	30	0.11			0.100%	0.120%										
E:Q114	3Q120	1	1/0	1	710	55.99	56	136	56	8	1, PEI/20kW	200	100	0.56			0.050%	0.089%										

